Int. J. Electrochem. Sci., 12 **(2017)** 2173 – 2183, doi: 10.20964/2017.03.07

International Journal of
ELECTROCHEMICAL
SCIENCE
www.electrochemsci.org

Preparation of Manganese Oxide/Graphene Aerogel and Its Application as an Advanced Supercapacitor Electrode Material

Xia Qiu[1], *Danyan Xu*[1],*Ling Ma*[2] *and Yong Wang*[3,*]

[1] College of Electrical and Electronic Information Engineering, Hubei Polytechnic University, Huangshi, 435000, P.R.China
[2] College of Information Science and Engineering, Wuchang Shouyi University, Wuhan, 430000, P.R.China
[3] HuangShi Central Hospital, Edong Healthcare, Huangshi, 435000, P.R.China
[*]E-mail: yongwang_hpu@qq.com

Received: 18 November 2016 / *Accepted:* 29 December 2016 / *Published:* 12 February 2017

Electrochemical supercapacitors (ECs) with high energy density and power capability have demonstrated promising potential in various energy applications. In this study, 3D MnO_2/rGO aerogels with excellent electrical conductivity was successfully prepared with a simple hydrothermal method. The as-prepared 3D aerogels could be applied for constructing the electrode of supercapacitor directly without the demand of other additives. Asymmetric supercapacitors were then constructed with Na_2SO_4 aqueous solution as electrolyte, MnO_2/rGO aerogel and rGO aerogel as positive and negative electrode, respectively. The asymmetric supercapacitor demonstrated maximum energy density of 18.2 Wh/kg with power density of 400 W/kg and excellent cycle stability as well.

Keywords: Supercapacitor; Aerogel; Graphene; Manganese oxide; Hydrothermal

1. INTRODUCTION

Development of renewable energy resources has attracted wide attention due to the energy crisis and environmental pollution. As a result, wind and solar energy have been developed rapidly in recent years to alleviate the energy demand. In addition, all-electric vehicles (EVs) or hybrid electric vehicles (HEVs) with low CO_2 emissions have aroused tremendous interest as well. As to variable wind/solar energy and battery-powered EVs/HEVs, electrochemical energy storage systems such as electrochemical capacitors (ECs), fuel cells and rechargeable batteries are of great importance. As shown from the Ragone plot (i.e., power density in function of energy density) of electrochemical energy storage systems [1], ECs with high power capacity and acceptable energy density are effective

solution for growing number of energy applications. Actually, the energy storage process for ECs can be divided into two types: non-Faradaic (capacitive) process on the basis of charge separation at the interface of electrode and electrolyte, and Faradaic (pseudocapacitive) process based on the occurrence of redox reactions on electrode. The active electrode materials with wide applications mainly composed of conductive polymers, carbon and transition metal oxides [2-8]. Manganese oxides have demonstrated promising potential as electrode materials in the application of ECs due to their numerous advantages such as high specific capacitance, environment friendly and low cost.

Lee and Goodenough firstly reported the pseudocapacitive behavior of manganese oxide in 1999 [9, 10]. Soon afterwards, a lot of research work had been carried out in the field of manganese oxide electrodes. It has been found that the occurrence of Faradic reaction either in the bulk or on the surface of electrodes constructed by manganese oxides was the major charge storage mechanism. The adsorption of electrolyte cations including Li^+, Na^+, K^+ and H^+ on the surface of manganese oxides was very important for the surface Faradaic reaction [11, 12].

Nevertheless, the capacitance of MnO_2 is relatively low owing to its low BET surface area and poor conductivity and the specific capacitance value was around 150-250 F/g [13]. Therefore, a hybrid electrode architecture that composed of MnO_2 film on various conductive supports with high BET surface area such as carbon nanotubes (CNTs), carbon nanofoams and mesoporous carbon was proposed for the sake of improving the electrochemical performance of MnO_2 electrode [14-17]. For the preparation of MnO_2/carbon composite, a lot of synthetic methods including physical mixing [18], electrodeposition [19], ball milling [20], thermal decomposition [21], sonochemical synthesis [22, 23], sol-gel reduction reaction [24] have been reported. Among the above-mentioned methods, the most attractive technique was the reduction method due to its self-limiting character. Specifically, the permanganate in aqueous solution was firstly reduced to insoluble manganese oxide by surface carbon, and then a thin film was formed on the surface of carbon by the deposition of obtained manganese oxide. However, the amount of MnO_2 deposited on carbon surface was relatively low (usually less than 64 wt.%), leading to the limited capacitance of MnO_2/carbon composites with the highest value 250 F/g [25]. Meanwhile, the retention ratio of capacitance was remarkably poor [26-28].

Recently, graphene materials have demonstrated promising potential in the application of electrochemical double-layer capacitors (EDLCs) owing to the remarkable capacitance (135 F/g) [29]. The large surface area is resulted not from the distribution of pores in solid but from the individual sheet itself. In addition, the overall high electrical conductivity can be preserved owing to the easy approach of electrolyte to the surface of graphene materials. Moreover, owing to the special two-dimensional (2D) structure of graphene, its capacitance can be greatly improved while maintaining remarkable electrochemical performance, leading to both highly reversible pseudocapacitance and electrochemical double-layer capacitance [30, 31].

In this study, MnO_2/reduced graphene oxide (MnO_2/rGO) aerogels with 3D interconnected networks have been prepared by a unique technique through soaking MnO_2/rGO hydrogels in ammonia solution. The obtained MnO_2/rGO aerogels exhibited unique microstructure, high mechanical strength and enhanced electrochemical performance as well. Furtherly, the obtained MnO_{23}/rGO aerogels was employed as positive electrode for the construction of asymmetric supercapacitor with rGO aerogel (GA) as negative electrode. The as-prepared asymmetric

supercapacitor demonstrates satisfactory high energy density, power density and excellent cycling stability.

2. EXPERIMENTAL

2.1. Materials

All chemicals used throughout the entire experiments were analytical reagents. A simple precipitation method was employed for the synthesis of amorphous MnO_2. Specifically, $KMnO_4$ solution was added drop by drop into Na_2SO_3 solution at room temperature. The modified Hummers method was used for the preparation of graphite oxide (GO) and the used raw material was powder graphite (99.95%, 1.3 μm, Aladdin) [32].

2.2. 3D graphene hydrogels and MnO_2/rGO hydrogels preparation

A controlled hydrothermal method was used for the preparation of 3D graphene hydrogels. Specific for, 60 mL of GO aqueous solution (1.5 mg/mL) was added to Teflon autoclave and then heated at 150 °C for 12 h.

As to the synthesis of MnO_2/rGO hydrogels, 90 mg of nano-MnO_2 was added into 60 mL of GO aqueous solution (1.5 mg/mL), and then the mixture was treated with ultrasonication for 60 min. After that, the homogeneous solution was added into Teflon autoclave and heated at 150 °C for 12 h. After the temperature of autoclave was cooled to room temperature naturally, the solution was treated with centrifugation and the obtained black solid was 3D MnO_2/rGO hydrogel.

2.3. Preparation of 3D graphene hydrogels and MnO_2/rGO aerogels

The graphene aerogel and MnO_2/rGO aerogel with high mechanical strength were prepared via hydrothermal method. Take graphene aerogel as example, the specific experimental procedure was as follows: the obtained graphene hydrogel was treated with ammonia solution with the volume content of 25%~28% at 90 °C for 1 h, and then freeze-dried.

2.4. Characterizations

Powder X-ray diffraction (PXRD) patterns of as-synthesized samples were performed on Bruker D8 ADVANCE with Cu Kα radiation. Scanning electron microscopy (SEM, HITACHI S-4800) was employed for investigating the morphology feature of as-synthesized samples. High-resolution X-ray photoelectron spectrometer (XPS, PHI Quantera SXM, ULVAC-PHI) was used for the determination of chemical bonds of graphene and MnO_2/rGO aerogels. Electronic analytical balance with the accuracy of 100 μg was applied for testing the weight of samples and the same sample was tested more than 3 times to ensure accuracy.

2.5. Electrochemical measurements

An electrochemical workstation with three-electrode system composed of graphene aerogel or MnO_2/rGO aerogel as working electrode, Pt coil as counter electrode and Ag/AgCl as reference electrode was employed for CV and galvanostatic charge/discharge measurements. Specific experimental parameters were set as follows: 0.5 M Na_2SO_4 (Showa, 99 %) solution as electrolyte, 0-0.9 V as potential window, different values (25, 100, 500 or 1000 mV/s) and (1, 10 or 50 A/g) as scan rates and current densities, respectively. The specific capacitance (*Cs*) can be calculated from CV loops:

$$Cs = (\int IdV)(vm\Delta V)^{-1}$$

where *I* represents current density (A/cm), υ the scan rate (V/s), *m* the mass of active MnO_2 (g) and ΔV the width of the potential window (V). The CV loop obtained at negative scans was used for the integration.

3. RESULTS AND DISCUSSION

It was difficult for the amorphous nano-MnO_2 in water to form stable suspension after ultrasound owing to precipitation and aggregation. However, the nano-MnO_2 particles can easily form stable solution via the help of GO with numerous oxygen containing functional groups. MnO_2 crystals with tunnel structures were assembled by octahedral [MnO_6] which is formed by one manganese atom with six surrounding oxygen atoms. Owing to plenty of attachment sites provided by a large amount of oxygen atoms on the large surface area of GO, the adsorption of nano-MnO_2 on the surface of GO sheets via hydrogen bonds was quiet easy and thus the stable GO/MnO_2 suspensions was successfully prepared.

The self-assembly process involves deoxygenization of GO, formation of $MnCO_3$ and transformation of MnO_2 was employed for the preparation of MnO_2/rGO hydrogel. As can be seen from the XRD patterns of GO (Fig. 1A), a sharp peak appeared at around $2\theta = 11.38°$, which could be ascribed to the (002) lattice plane of GO. The calculated interlayer distance of GO (0.724 nm) was far higher than that of graphite (0.318 nm), which could be resulted from the insertion of oxygen-containing groups into graphite layers. As can be seen from the XRD pattern of rGO, a broad peak at $2\theta = 23.3°$ appeared after reduction. The interlayer distance of rGO (0.38 nm) was higher than that of graphite (0.336 nm), indicating the successful synthesis of graphene from GO.

XRD patterns of MnO_2 nanorods (NRs) and $MnCO_3$ nanoparticles (NPs) that synthesized by hydrothermal method were shown in Fig. 1B. As shown form the broad and weak peaks, the raw MnO_2 was amorphous. Then MnO_2 turned to crystal structure with long nano-rod morphology after hydrothermal treatment for 12 h. The as-synthesized MnO_2 crystal was in the tetragonal phase of α-MnO_2 (JCPDS No.44-0141) as concluded form the diffraction peaks. Furtherly, the formation of $MnCO_3$ (PDF NO.44-1472) was affirmed with the XRD pattern. $MnCO_3$ NPs could be prepared through the reaction between MnO_2 and oxygen-containing functional groups of GO nanosheets at high temperatures and pressures.

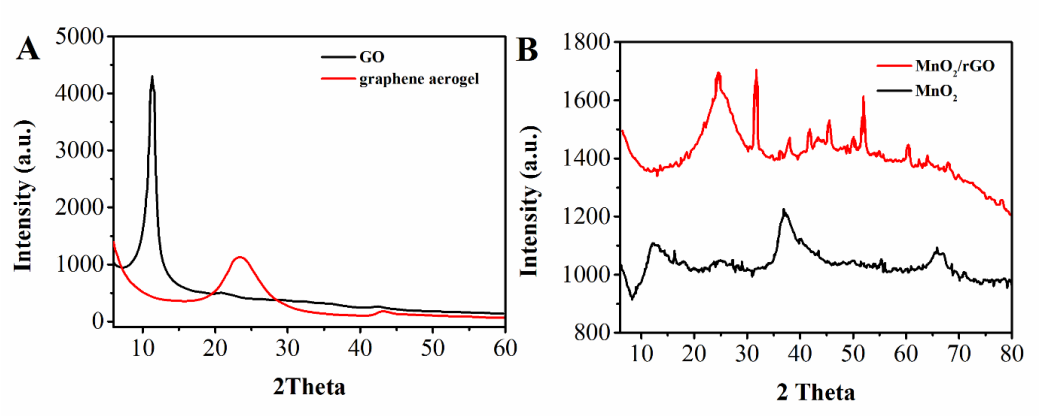

Figure 1. XRD patterns of (A) GO and graphene aerogel, and (B) MnO_2/rGO aerogel and MnO_2.

The XPS spectra of GO and graphene aerogel were shown in Fig. 2A. Obviously, the O1s intensity of GO was reduced drastically, indicating the oxygen content of GO changed from 34 to 5 % in the thermal reduction process to form graphene sheet. For further comparison, Fig. 2B and 2C showed the enlarged C1s signals. It was found that double peak with a shoulder on the right of second peak appeared in the C1s signal of graphite oxide. In contrast, a single peak with two shoulders on the right was found in the C1s signal of graphene aerogel. The C1s signal can be de-convoluted into four constituent peaks located at 288.6, 287.8, 286.8 and 284.7 eV, which belonged to carboxyl groups, carbonyl groups, epoxide or hydroxyl groups and C-C or C=C of aromatic rings, respectively [33, 34]. It was affirmed that the oxygen-containing functional groups of graphite oxide has been greatly reduced in the thermal reduction process by comparing Fig. 2B and 2C. In addition, the binding energy of C-C and C=C of aromatic rings was slightly shifted to lower values because that strong electron-drawing element O was removed from the basal plane.

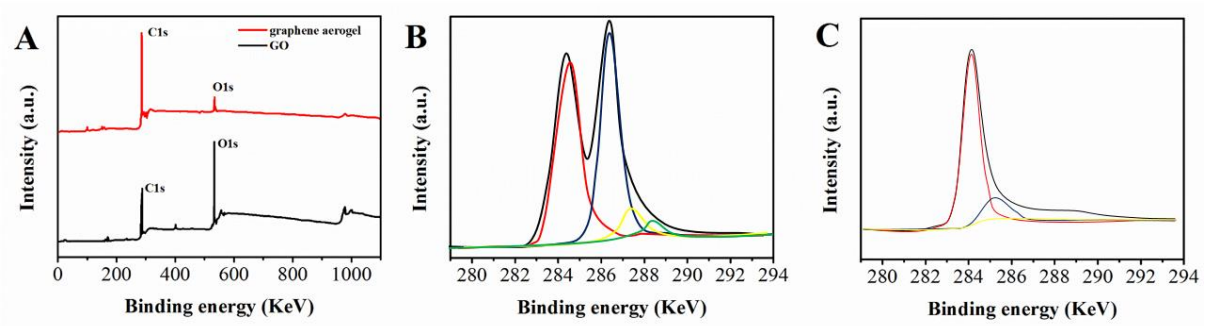

Figure 2. (A) XPS spectra for C and O in GO and graphene aerogel. XPS spectra of C1s for (B) GO and (C) graphene aerogel.

As can be seen form the SEM image of graphene aerogel (Fig. 3A), 3D porous structure with well-connected thin sheets was observed. As show form the SEM image of MnO_2/rGO aerogel (Fig. 3B), MnO_2 nanostructure was deposited within the graphene aerogel. Maintenance of the 3D structure for the graphene networks, with no cracks or collapsing owing to the strength. Reduction of the size of

the pores and the thickness of the foam, which results in a lower volume for the 3D graphene network. The improvement of the flexibility of the 3D graphene network and its ability to suffer a large deformation; allowing a uniform electrodeposition of the MnO_2 nanostructure material on the 3D graphene network by shortening the diffusion distance of the solution, due to its hydrophobic property [35].

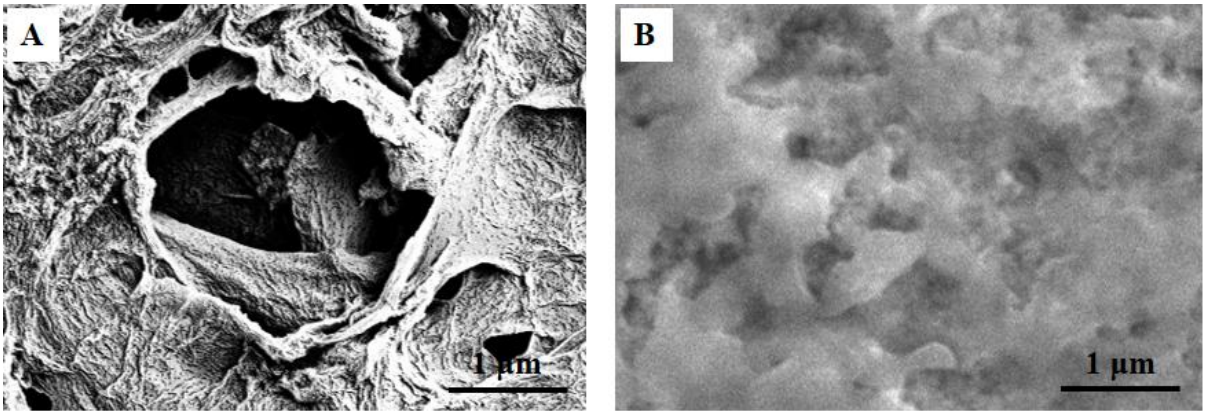

Figure 3. SEM images of (A) graphene aerogel and (B) MnO_2/rGO aerogel.

The electrochemical performance of as-synthesized graphene and MnO_2/rGO aerogel was investigated and the results were shown in Fig. 4. All electrochemical experiments were performed in a three-electrode system with 1 M Na_2SO_4 as electrolyte and -0.2 V~0.8 V as scan potential. Cyclic voltammetry (CV) curves obtained on MnO_2/rGO aerogel and graphene aerogel electrodes with various scan rates were shown in Fig. 4A and B, respectively. When the scan rate was less than 20 mV/s, all CV curves were found to be nearly ideal symmetrical rectangular shape, suggesting the remarkable capacitive behavior. However, when the scan rate exceeded 100 mV/s, the shape of CV curves exhibited slightly deviation from rectangular, which could be resulted from the difficulty for ions in approaching the deep pores. In contrast to the rectangular shape of CV curves obtained on MnO_2/rGO aerogel electrode, the CV curves obtained on graphene aerogel electrode were much closer to quasi-rectangular shape. The different shapes are mainly derived from the faradaic pseudocapacitance of MnO_2/rGO aerogel.

Fig. 4C showed the specific capacitance of graphene aerogel and MnO_2/rGO aerogel electrodes in function of scan rates (5-100 mV/s). For both graphene aerogel electrode and MnO_2/rGO aerogel electrode, highest capacitances were obtained at scan rate of 5 mV/s and the values were 116.8 and 204.6 F/g, respectively. In addition, the capacitance of MnO_2/rGO aerogel was 81 F/g at the scan rate of 100 mV/s, demonstrating that 39% of capacitance was retained. The galvanostatic charge/discharge curves obtained on graphene aerogel and MnO_2/rGO aerogel electrodes at constant current density of 1 A/g were given in Fig. 4D. The existence of this critical value may be because the thickness of MnO_2 corresponding to the critical mass is close to the Na^+ diffusion length at these scan rates for this particular graphene/MnO_2 composite electrode [36, 37]. Obviously, the capacitance obtained on MnO_2/rGO aerogel electrode was higher than that obtained on graphene aerogel electrode. It was

found that the galvanostatic charge/discharge curve obtained on MnO_2/rGO aerogel electrode was slightly tortured, indicating that both pseudocapacity and double layer have made a contribution.

CV curves of graphene aerogel electrode at different scan rates were investigated with the potential ranging from -1.1 V to -0.2 V and the results were shown in Fig. 5A. Nearly rectangular shape was found for the graphene aerogel electrode, indicating the ideal capacitive behavior. Furtherly, CV curves of graphene aerogel and MnO_2/rGO aerogel electrodes were measured at scan rate of 20 mV/s and the results were shown in Fig. 5B.

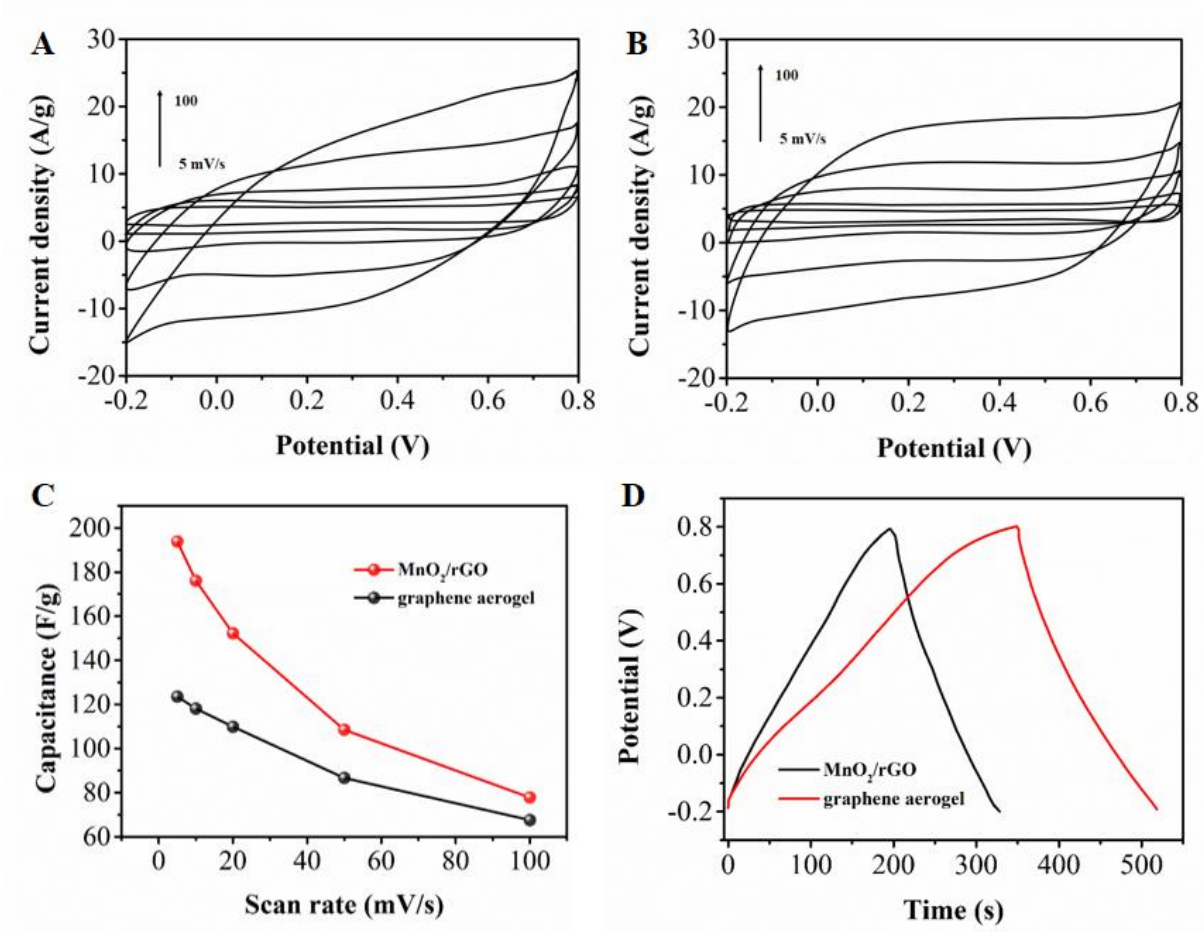

Figure 4. CV curves obtained on electrodes constructed with (A) MnO_2/rGO aerogel and (B) graphene aerogel at different scan rates. (C) Specific capacitance of graphene aerogel and MnO_2/rGO aerogel electrodes in function of scan rates. (D) Galvanostatic charge/discharge curves of graphene aerogel and MnO_2/rGO aerogel electrodes at constant current density of 1 A/g.

For graphene aerogel electrode, the scanning potential range was between -1 and -0.2 V. In contrast, the scanning potential range of MnO_2/rGO aerogel electrode was between -0.2 to 0.8 V. Subsequently, asymmetric supercapacitors with MnO_2/rGO aerogel as positive electrode and graphene aerogel as negative electrode were constructed. It was worth noting that the charge balance between positive electrode (q_+) and negative electrode (q_-) was required for asymmetric supercapacitors owing to the different capacitance of graphene aerogel and MnO_2/rGO aerogel. The mass of MnO_2/rGO aerogel (m_+) and graphene aerogel (m_-) could be determined by the following Equation.

$$\frac{m_+}{m_-} = \frac{Sc_- \times \Delta E_-}{Sc_+ \times \Delta E_+}$$

The specific capacitance values (SC) and potential windows (ΔE) could be acquired from Fig. 5B. Thus, the obtained optimal mass ratio of graphene aerogel and MnO_2/rGO aerogel is about 0.55.

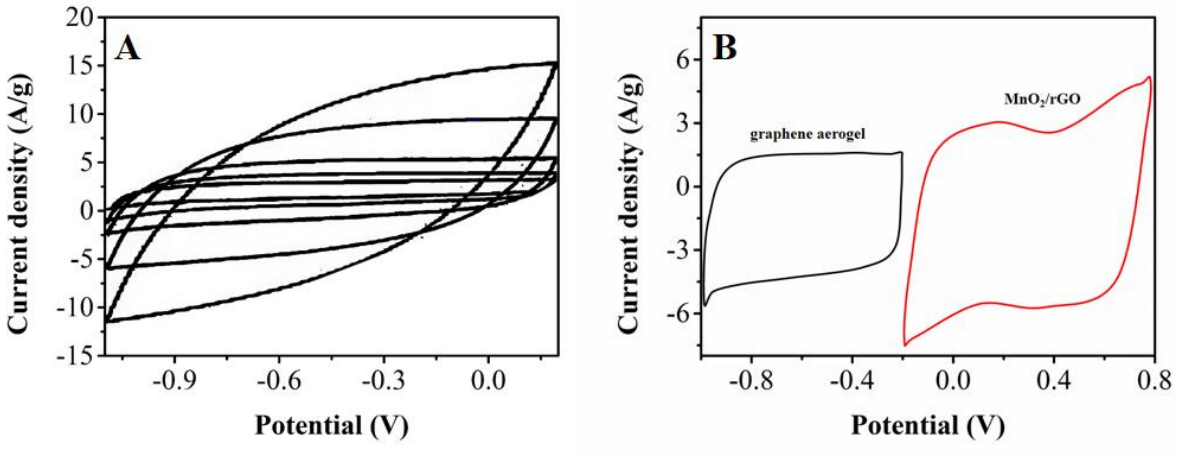

Figure 5. (A) CV curves of graphene aerogel electrode under various scan rates with the potential ranging from -1.1 V to -0.2 V. (B) CV curves of graphene aerogel and MnO_2/rGO aerogel electrodes at scan rate of 20 mV/s.

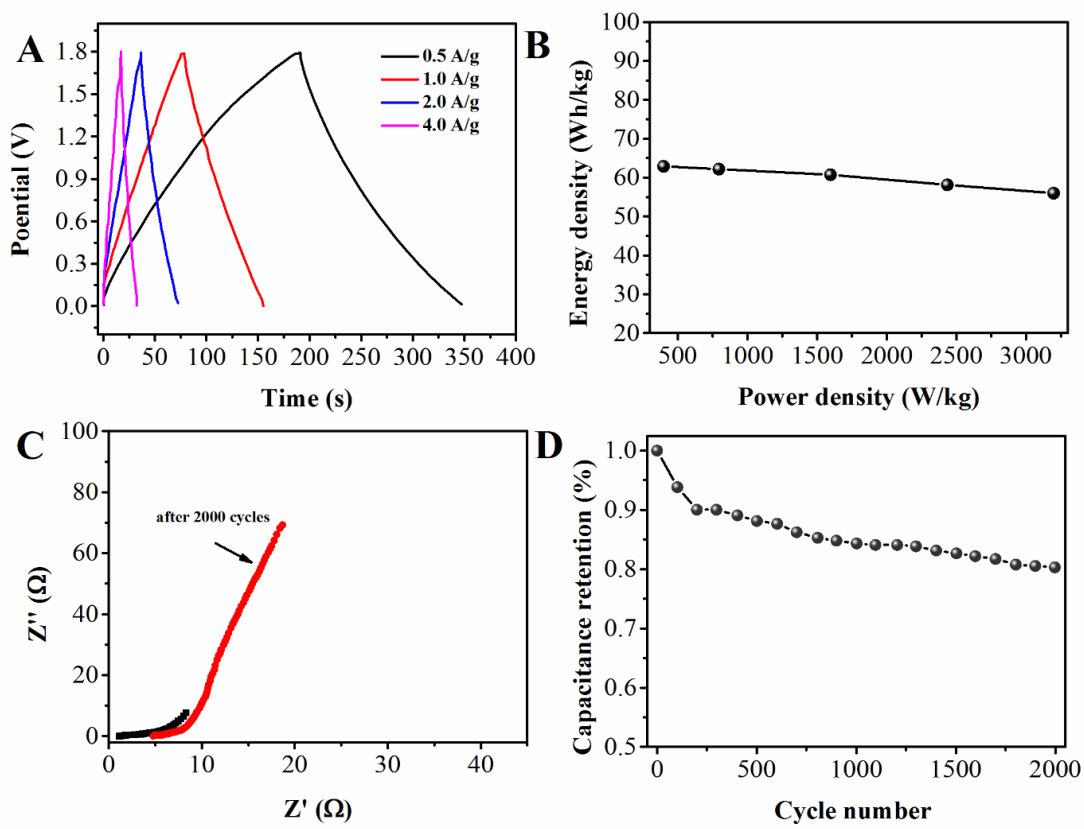

Figure 6. (A) Galvanostatic charge/discharge curves of the as-prepared asymmetric supercapacitor at under various current densities. (B) Ragone plots, (C) Nyquist plot and (D) Cycle life of as-prepared asymmetric supercapacitor.

The electrochemical performance of the resulting asymmetric supercapacitor was investigated at constant potential of 1.6 V and the results were shown in Fig. 6. As can be seen from the galvanostatic charge/discharge curves under vatious current densities (Fig. 6A), all curves exhibited high symmetry with little voltage (IR) drop, suggesting excellent reversibility with low internal resistance. The obtained specific capacitance at current densities of 0.5,1, 2 and 4 A/g was 62.9, 62.18, 60.73 and 58.24 F/g, respectively. As shown from the Ragone plots (Fig. 6B), the maximum energy density was 18.2 Wh/kg with power density of 400 W/kg. These values are superior to the similar previously reported symmetrical systems. Table 1 shows the maximum energy density comparison of our proposed materials with other literatures.

Table 1. Maximum energy density comparison of our proposed MnO_2/rGO aerogel with other reports

Material	Maximum energy density (Wh/kg)	Reference
Prussian Blue modified positive electrode	7.68	[38]
Activated-N-doped graphene	66	[39]
GO/PPy	15	[40]
Papers coated with carbon nanotubes	41	[41]
$Ni(OH)_2$/Graphene	77.8	[42]
MnO_2/rGO	18.2	This work

As shown form the Nyquist plot (Fig. 6C), a straight line and an arc line was observed in the low and high frequency region, respectively, suggesting ideal capacitive behavior. The charge transport resistance was small, which could be deduced from the small arc in the low frequency region. The equivalent series resistances (ESR) of the electrodes after 2000 cycles were calculated to be 8 Ω by extrapolating the straight line to intersect the real axis. Fig. 6D showed the cycle life of as-prepared asymmetric supercapacitor at current density of 1.2 A/g. It was found that about 79.8% of the specific capacitance could be remained after 2000 cycles, indicating the excellent cycle stability of as-prepared asymmetric supercapacitor. In general, owing to the synergistic effects of graphene nanosheets and MnO_2, the freestanding and robust MnO_2/rGO aerogel exhibits excellent electrochemical performance (high energy density and power capability and excellent stability), demonstrating promising potential in the application of flexible energy devices.

4. CONCLUSION

In conclusion, MnO_2/rGO aerogel with the decoration of MnO_2 nanorods onto graphene sheets was successfully synthesized via a hydrothermal method. The obtained nanohybrid aerogel was highly conductive with highest capacitance of 204.6 F/g. The asymmetric supercapacitor constructed with the obtained MnO_2/rGO aerogel exhibited high energy density and excellent stability. In addition, the

proposed simple and green synthetic method herein can also be applied for the preparation of other transitional metal oxide/graphene aerogel.

References

1. P. Simon and Y. Gogotsi, *Nature materials*, 7 (2008) 845.
2. J. Zheng and T. Jow, *Journal of The Electrochemical Society*, 142 (1995) L6.
3. P. Soudan, J. Gaudet, D. Guay, D. Bélanger and R. Schulz, *Chemistry of materials*, 14 (2002) 1210.
4. B. Conway, V. Birss and J. Wojtowicz, *Journal of Power Sources*, 66 (1997) 1.
5. P.A. Nelson and J.R. Owen, *Journal of The Electrochemical Society*, 150 (2003) A1313.
6. C. Lin, J.A. Ritter and B.N. Popov, *Journal of the Electrochemical Society*, 145 (1998) 4097.
7. N.-L. Wu, S.-Y. Wang, C.-Y. Han, D.-S. Wu and L.-R. Shiue, *Journal of Power Sources*, 113 (2003) 173.
8. N.-L. Wu, *Mater. Chem. Phys.*, 75 (2002) 6.
9. H.Y. Lee and J.B. Goodenough, *J. Solid State. Chem.*, 144 (1999) 220.
10. L. Si-Heng, L. Qing-He, Q. Li, L. Le-Hui and W. Hong-Yu, *Chinese Journal of Analytical Chemistry*, 40 (2012) 339.
11. M. Toupin, T. Brousse and D. Bélanger, *Chemistry of Materials*, 16 (2004) 3184.
12. S.C. Pang, M.A. Anderson and T.W. Chapman, *Journal of the Electrochemical Society*, 147 (2000) 444.
13. T. Brousse and D. Bélanger, *Electrochemical and solid-state letters*, 6 (2003) A244.
14. A. Sumboja, C.Y. Foo, X. Wang and P.S. Lee, *Adv. Mater.*, 25 (2013) 2809.
15. B. Wei, L. Wang, Q. Miao, Y. Yuan, P. Dong, R. Vajtai and W. Fei, *Carbon*, 85 (2015) 249.
16. C. Ng, H. Lim, Y. Lim, W. Chee and N. Huang, *International Journal of Energy Research*, 39 (2015) 344.
17. V. Sahu, S. Grover, B. Tulachan, M. Sharma, G. Srivastava, M. Roy, M. Saxena, N. Sethy, K. Bhargava and D. Philip, *Electrochimica Acta*, 160 (2015) 244.
18. E. Raymundo-Pinero, V. Khomenko, E. Frackowiak and F. Beguin, *Journal of the Electrochemical Society*, 152 (2005) A229.
19. C.Y. Lee, H.M. Tsai, H.J. Chuang, S.Y. Li, P. Lin and T.Y. Tseng, *Journal of the Electrochemical Society*, 152 (2005) A716.
20. Y. Zhou, B. He, F. Zhang and H. Li, *Journal of Solid State Electrochemistry*, 8 (2004) 482.
21. Z. Fan, J. Chen, M. Wang, K. Cui, H. Zhou and Y. Kuang, *Diamond and related materials*, 15 (2006) 1478.
22. A. Zolfaghari, F. Ataherian, M. Ghaemi and A. Gholami, *Electrochimica Acta*, 52 (2007) 2806.
23. H. Kawaoka, M. Hibino, H. Zhou and I. Honma, *Journal of power sources*, 125 (2004) 85.
24. M. Hibino, H. Kawaoka, H. Zhou and I. Honma, *Electrochimica acta*, 49 (2004) 5209.
25. X. Jin, W. Zhou, S. Zhang and G.Z. Chen, *Small*, 3 (2007) 1513.
26. X. Xie and L. Gao, *Carbon*, 45 (2007) 2365.
27. J. Yan, Z. Fan, T. Wei, W. Qian, M. Zhang and F. Wei, *Carbon*, 48 (2010) 3825.
28. Y. Wang and I. Zhitomirsky, *Langmuir*, 25 (2009) 9684.
29. M.D. Stoller, S. Park, Y. Zhu, J. An and R.S. Ruoff, *Nano letters*, 8 (2008) 3498.
30. D.-W. Wang, F. Li, J. Zhao, W. Ren, Z.-G. Chen, J. Tan, Z.-S. Wu, I. Gentle, G.Q. Lu and H.-M. Cheng, *ACS nano*, 3 (2009) 1745.
31. J. Yan, T. Wei, B. Shao, Z. Fan, W. Qian, M. Zhang and F. Wei, *Carbon*, 48 (2010) 487.
32. W. Chen, L. Yan and P.R. Bangal, *Carbon*, 48 (2010) 1146.
33. J. Zhang, H. Yang, G. Shen, P. Cheng, J. Zhang and S. Guo, *Chemical Communications*, 46 (2010) 1112.
34. O.C. Compton, D.A. Dikin, K.W. Putz, L.C. Brinson and S.T. Nguyen, *Adv. Mater.*, 22 (2010) 892.

35. Y. He, W. Chen, X. Li, Z. Zhang, J. Fu, C. Zhao and E. Xie, *ACS nano*, 7 (2012) 174.
36. J. Lin, Y. Zheng, Q. Du, M. He and Z. Deng, *Nano*, 8 (2013) 1350004.
37. L. Sheng, L. Jiang, T. Wei and Z. Fan, *Small*, 12 (2016) 5217.
38. P. Díaz, Z. González, R. Santamaría, M. Granda, R. Menéndez and C. Blanco, *Electrochimica Acta*, 212 (2016) 848.
39. Q. Fan, M. Yang, Q. Meng, B. Cao and Y. Yu, *Journal of The Electrochemical Society*, 163 (2016) A1736.
40. A. Singh and A. Chandra, *Journal of Applied Electrochemistry*, 43 (2013) 773.
41. Y.J. Kang, H. Chung, C.-H. Han and W. Kim, *Nanotechnology*, 23 (2012) 065401.
42. J. Yan, Z. Fan, W. Sun, G. Ning, T. Wei, Q. Zhang, R. Zhang, L. Zhi and F. Wei, *Adv Funct Mater*, 22 (2012) 2632.